Editors' Suggestion

Genuine 12-Qubit Entanglement on a Superconducting Quantum Processor

Ming Gong,[1,2] Ming-Cheng Chen,[1,2] Yarui Zheng,[1,2] Shiyu Wang,[1,2] Chen Zha,[1,2] Hui Deng,[1,2] Zhiguang Yan,[1,2] Hao Rong,[1,2] Yulin Wu,[1,2] Shaowei Li,[1,2] Fusheng Chen,[1,2] Youwei Zhao,[1,2] Futian Liang,[1,2] Jin Lin,[1,2] Yu Xu,[1,2] Cheng Guo,[1,2] Lihua Sun,[1,2] Anthony D. Castellano,[1,2] Haohua Wang,[3] Chengzhi Peng,[1,2] Chao-Yang Lu,[1,2] Xiaobo Zhu,[1,2] and Jian-Wei Pan[1,2]

[1]*Hefei National Laboratory for Physical Sciences at Microscale and Department of Modern Physics, University of Science and Technology of China, Hefei, Anhui 230026, China*

[2]*Shanghai Branch, CAS Center for Excellence and Synergetic Innovation Center in Quantum Information and Quantum Physics, 10 University of Science and Technology of China, Shanghai 201315, China*

[3]*Department of Physics, Zhejiang University, Hangzhou, Zhejiang 310027, China*

(Received 6 November 2018; published 20 March 2019)

We report the preparation and verification of a genuine 12-qubit entanglement in a superconducting processor. The processor that we designed and fabricated has qubits lying on a 1D chain with relaxation times ranging from 29.6 to 54.6 μs. The fidelity of the 12-qubit entanglement was measured to be above 0.5544 ± 0.0025, exceeding the genuine multipartite entanglement threshold by 21 statistical standard deviations. After thermal cycling, the 12-qubit state fidelity was further improved to be above 0.707 ± 0.008. Our entangling circuit to generate linear cluster states is depth invariant in the number of qubits and uses single- and double-qubit gates instead of collective interactions. Our results are a substantial step towards large-scale random circuit sampling and scalable measurement-based quantum computing.

DOI: 10.1103/PhysRevLett.122.110501

Quantum entanglement is a highly nonclassical aspect of quantum mechanics [1,2], and a central resource to quantum information sciences [3–6]. A stringent benchmark for high-precision control of multiple quantum systems is the ability to create a genuine multipartite entangled (GME) state that cannot be expressed as a biseparable state or mixture of biseparable states with respect to variable partitions [7]. So far, GME states in the form of Greenberger-Horne-Zeilinger (GHZ) states have been reported with 10 superconducting qubits [8], 14 trapped ions [9], and 18 photonic qubits [10]. We note that in several other experiments involving large numbers of qubits [11–15], the presence of genuine entanglement for more than 5 qubits has not been verified. Here, we report the creation and verification of a 12-qubit linear cluster (LC) state, the largest GME state reported in solid-state quantum systems. LC states are robust against noise, and serve as a universal resource for one-way quantum computing [16,17]. Our approach does not rely on collective interactions to create GME as in the previous work [8,9], but is based on individual single-qubit gates and controlled-phase (CZ) entangling gates, which makes our approach scalable to larger numbers of qubits and applicable to random quantum circuit sampling demonstrations of quantum supremacy [18].

An N-qubit cluster state is a simultaneous eigenstate of N commuting Pauli stabilizer operators with eigenvalues all equal to $+1$ [16]. Stabilizer operators consist of nearest-neighbor interactions of qubits arranged in lattices. The simplest example is a linear cluster (LC) state, where stabilizer operators s_i are defined on a qubit chain as

$$s_i = \sigma_Z^{(i-1)}\sigma_X^{(i)}\sigma_Z^{(i+1)}. \tag{1}$$

$\sigma_X^{(i)}$ and $\sigma_Z^{(i)}$ are Pauli X and Z operators on the ith qubit, respectively (and at the boundary $\sigma_Z^{(0)}$ and $\sigma_Z^{(N+1)}$ are idle). Cluster states can be prepared either by cooling a nearest-neighbor Ising-type Hamiltonian $H = \sum_{i=1}^{N}(1 - s_i/2)$ system to its ground state or by dynamically implementing a set of CZ gates,

$$|\mathrm{LC}_N\rangle = \left(\prod_{i=1}^{N-1}\mathrm{CZ}^{(i,i+1)}\right)|+\rangle^{\otimes N}, \tag{2}$$

on a qubit lattice initialized in the $|+\rangle = (|0\rangle + |1\rangle)/\sqrt{2}$ state. In this work, we use the latter method on a superconducting quantum processor by implementing the gate sequence shown diagrammatically in Fig. 2(a).

As can also be seen in Fig. 1(a), the processor has 12 transmon qubits [19] of the Xmon variety [20]. Each qubit has a microwave drive line (XY), a fast flux-bias line (Z) and a readout resonator. The qubits are arranged in a line with neighboring qubits coupled capacitively. All the readout resonators are coupled to a common transmission line for joint readout of the qubit states. The Hamiltonian of the 12-qubit system is given by

$$H/\hbar = \sum_{i=1}^{12}\omega_i\hat{n}_i + \frac{\eta_i}{2}\hat{n}_i(\hat{n}_i - 1) + \sum_{i=1}^{11} g_i(\hat{a}_i^\dagger\hat{a}_{i+1} + \hat{a}_i\hat{a}_{i+1}^\dagger), \tag{3}$$

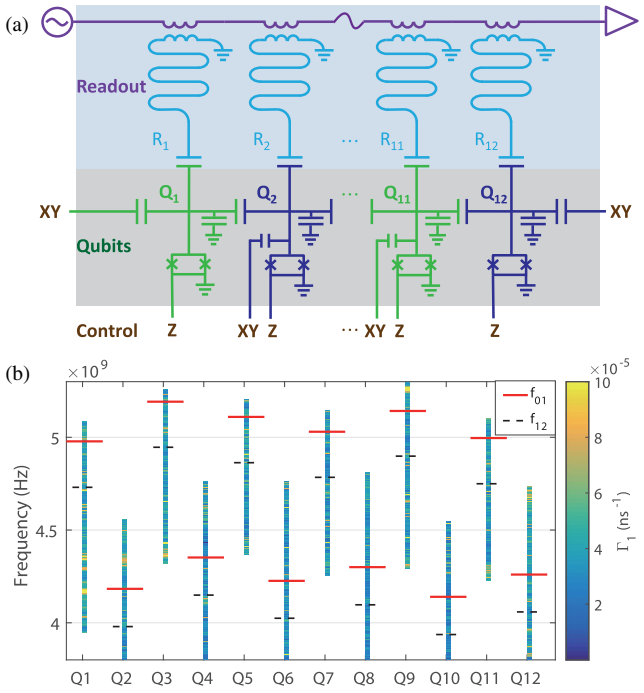

FIG. 1. (a) Circuit diagram. There are 12 neighboring qubits illustrated in two colors (green/dark blue) that correspond to two groups of working frequencies. The green ones are around 5 GHz and the dark-blue ones are around 4.2 GHz. All readout resonators (light blue) are coupled to a common transmission line (purple). By using frequency-domain multiplexing, joint readout for all qubits can be performed. For each qubit, individual capacitively coupled microwave control lines (XY) and inductively coupled bias lines (Z) enable full control of qubit operations. (b) The idling frequencies of both f_{01} (solid red line) and f_{12} (dotted black line) for all qubits. The color of the vertical bars on qubit levels indicates the energy relaxation rate Γ_1. All qubit operations are performed within this frequency range.

where $\hat{n}$ is the number operator, $\hat{a^\dagger}$ ($\hat{a}$) is the creation (annihilation) operator, ω_i and η_i are the transition frequency and the anharmonicity of the ith qubit, respectively, and g_i is the interaction strength between ith and $(i+1)$th qubits. Each qubit transition frequency can be tuned by Z lines and single-qubit quantum gates can be implemented by driving the XY lines. For specific qubit properties, refer to the Supplemental Material [21].

The specific quantum circuit used to produce the LC state is illustrated in Fig. 2(a). To perform the entire operation, first we wait 300 μs to relax the qubits into the $|0\rangle$ state. Then, we apply $Y/2$ gates to rotate all the qubits into the $|+\rangle$ state. After that, 11 CZ gates are performed to entangle all 12 qubits. Finally, we measure all qubit states with a joint readout operation.

The nearest-neighbour coupling enables the application of "fast adiabatic" CZ gates [20]. To minimize the effects of decoherence and ZZ coupling between neighbouring qubits, we shorten the depth of the circuit by applying the CZ gates in parallel. The minimization of ZZ coupling also requires a large detuning between adjacent qubits. We carefully arranged the idle frequencies to avoid TLSs and adjust the frequency differences between adjacent qubits larger than 700 MHz. The idle frequencies for all relevant qubits are shown in Fig. 1(b). Choosing a gate sequence like this, along with carefully optimizing and calibrating the control pulses, was crucial to achieve this high fidelity entanglement. We have put the relevant technical details into the Supplemental Material [21].

The fidelities of the $Y/2$ gates and CZ gates are reported in Figs. 2(b) and 2(c), respectively. The fidelities of CZ gates are calculated using quantum process tomography (QPT), where maximum-likelihood estimation is used to construct physical density matrices resulting from an arbitrary input. The average CZ gate fidelity is 0.939. But it is also possible to characterize our gates for states initialized in $|++\rangle$, in which case the average fidelity increases to 0.956. This is more relevant to our experiment because CZ gates are only ever applied to the $|++\rangle$ state. The Q_2-Q_3 gate is the worst of all the CZ gates. This is caused by defects in the physical system located on Q_3 around 4.43 GHz and on Q_2 around 4.34 GHz, which appear in Fig. 1(b) as a dramatic increase of the relaxation rate in a narrow range of frequencies. These so-called two-level systems (TLS) cause a qubit state to leak out of the computational state space, limiting the gate fidelity. Ignoring Q_2 and Q_3, the rest of the qubits have an average gate and state fidelity which increase to 0.946 and 0.962, respectively.

The fidelities of the CZ gates characterized here are lower than the actual gate fidelities. This is partly because unlike randomized benchmarking (RB), our characterization process includes errors from state preparation and readout. Also, when we characterize a single entangling gate, we run the entire three-layer sequence, which makes the effects of decoherence and ZZ coupling larger due to the tripled length of the operation (192 ns). Fidelities of a single CZ gate for this processor, characterized by RB, typically exceed 0.99. However, optimizing the CZ gates by embedding them into the whole circuit is essential, otherwise a high-fidelity GME state is unobtainable.

Fidelity measurements of states produced in quantum information experiments are traditionally calculated from the state's density matrix, which is obtained from quantum state tomography (QST). This full characterization of a state requires measurements and computational resources that grow exponentially in the number of qubits. In this work, full characterization proves impractical, so we find a lower bound of the state fidelity using

$$\mathcal{F} \geq \vec{\alpha}_{XZ} P_{XZ} + \vec{\alpha}_{ZX} P_{ZX} - 1, \tag{4}$$

where P_{XZ} and P_{ZX} are probability distributions measured with $\sigma_{XZ\ldots XZ}$ and $\sigma_{ZX\ldots ZX}$ bases, and $\vec{\alpha}_{XZ}$ and $\vec{\alpha}_{ZX}$ are two

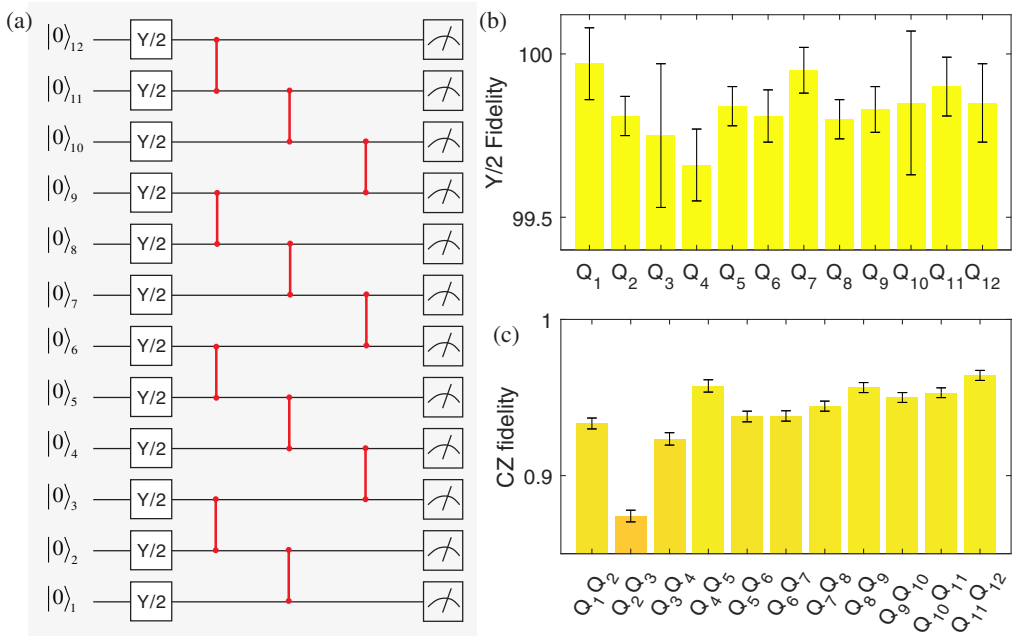

FIG. 2. (a) Algorithm to generate linear cluster state. The initial state for each qubit is $|0\rangle$. $Y/2$ gates are applied to bring each qubit to $|+\rangle$, then the CZ gates are applied to generate the GME state. Finally, joint measurements are performed to obtain the state fidelity. (b) The fidelities of $Y/2$ single qubit gates obtained by randomized benchmarking. The error bars represent a 95% confidence interval, determined from nonlinear least-squares fits. (c) CZ gate fidelities obtained by performing quantum process tomography. Error bars on the data are calculated via the bootstrapping method, with a 95% confidence interval.

sets of coefficients equal to the theoretical distribution times 2^6 ($N = 12$) [7,30,31]. See the Supplemental Material [21] for the justification of this bound.

The measured probability distributions, P_{XZ} and P_{ZX}, of the 12-qubit cluster state are shown in Figs. 3(a), 3(b), along with the theoretical distributions of the ideal state. The infidelity can be calculated from the sum of the small components in the measured P_{XZ} and P_{ZX} distributions. These values, which mainly come from the population imbalance and phase errors in the prepared states, do not interfere destructively in the measurement process.

In our experiments, the readout is a positive-operator valued measurement, and we use calibrated transition matrices to obtain the original distributions. Because of statistical fluctuations, small probability values may become negative. We note that the fidelity bound in this process is reliable (see the Supplemental Material [21]). We perform 250 000 projective measurements to construct the probability distributions P_{XZ} and P_{ZX}. The lower bound of the 12-qubit linear cluster state fidelity is calculated to be 0.5544 ± 0.0025. We also prepared other linear cluster states from 4 qubits to 11 qubits by initializing N neighboring qubits in $|+\rangle$ states and leaving the other qubits in $|0\rangle$ states. The fidelities are summarized in Fig. 3(c).

Once we have a lower bound of the state fidelity, we use entanglement witness to prove that the prepared states are genuinely entangled [7]. An arbitrary quantum state ρ that is biseperable will always have a fidelity $\mathrm{F} = \mathrm{Tr}(\rho|\mathrm{LC_n}\rangle\langle\mathrm{LC_n}|)$ less than 0.5; hence states with fidelity above 0.50 are genuinely entangled. Figure 3(c) shows that all states produced meet this criterion for entanglement. For the case of 12 qubits, the fidelity is 0.5544 ± 0.0025 and exceeds the threshold for entanglement by 21 statistical standard deviations. We note that a reported 16-qubit "full entanglement" [15] is not necessarily a *genuine multipartite entanglement* because it is possible to generate fully entangled states with classical mixtures of separable states. An example is given in the Supplemental Material [21].

Scalability is one of the key advantages of our system: any two linear cluster states can be combined to form a larger cluster state by applying one additional CZ gate. Additionally, a chain of N qubits (for $N > 4$) will always take three layers of CZ gates to create an LC state, so negative effects from decoherence and ZZ crosstalk will not be exacerbated by an increased circuit depth. We judge that using identical technology, a 20-qubit LC state could be created, if not for the presence of TLSs in the physical qubits. On our system, after the TLSs coupled to Q_2 and Q_3 successfully removed by thermal cycling, the 12-bit LC state fidelity is improved to higher than 0.7. For more discussion of TLSs, see the Supplemental Material [21]. TLSs are the most immediate obstacle towards scaling to larger systems, and more work needs to be done investigating their physical origins and devising methods to mitigate their effects on superconducting quantum processors.

The LC states produced in this work have immediate applications to near-term quantum supremacy experiments. Random quantum circuit sampling experiments typically

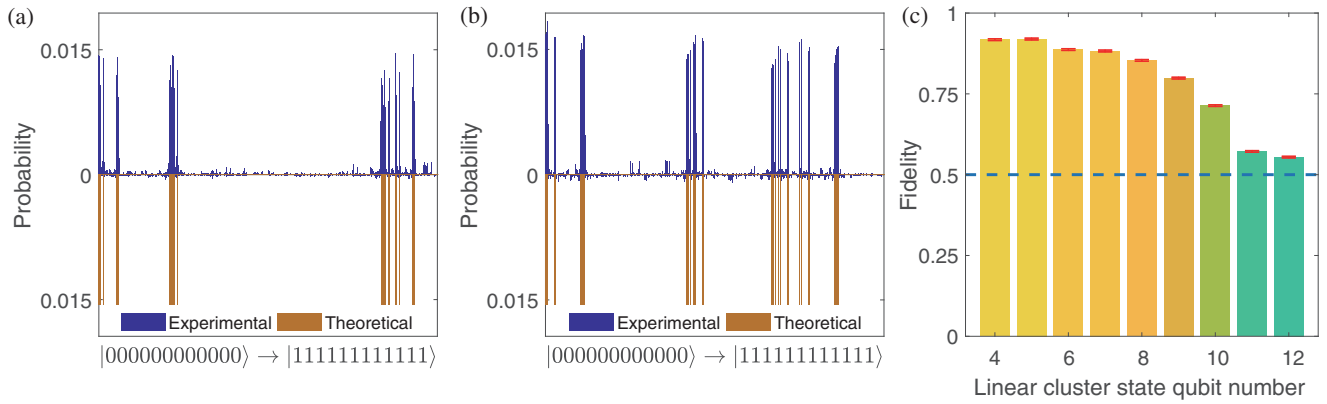

FIG. 3. (a) Experimental and theoretical distribution of the $XZ\ldots XZ$ component in the 12 qubit linear cluster state. (b) Same as (a), but use $ZX\ldots ZX$ instead. In both (a) and (b), the states are in the form of $|Q_{12}\ldots Q_1\rangle$. Experimental and theoretical results are presented in dark blue and brown, respectively. (c) Linear cluster state fidelities from 4 to 12 qubits, which are 0.9176(28), 0.9196(28), 0.8870(27), 0.8827(27), 0.8536(27), 0.7988(27), 0.7136(26), 0.5720(25), and 0.5544(25), exceed GME threshold by 149, 149, 143, 141, 130, 110, 82, 28, and 21 statistical standard deviations, respectively. State fidelities are calculated from two components, $XZ\ldots XZ$ and $ZX\ldots ZX$, of the linear cluster state. Error bars have a confidence interval of 95%, obtained from statistical calculation. A threshold of 50% for genuine entanglement is marked with a blue dashed line.

use gate sequences that alternate between randomly chosen single-qubit gates and entangling gates on qubits arranged in 1D or 2D lattices [18]. These gates are optimized individually using RB [20,32,33], but simultaneous implementation of the gates causes them to interfere with each other. Instead of standard 1- and 2-qubit gates, the cluster state production sequences in this work can also be used as building blocks for random quantum circuit sampling. The techniques demonstrated in this work, those of optimization of simultaneous gates, are well suited to address similar challenges posed by the random circuit sampling experiments.

In general, cluster states have notable applications and advantages. The most interesting application is probably one-way quantum computing, where the most common starting state is the cluster state. The complex structure of the cluster state entanglement makes it possible to generate every quantum state [17], which allows for further research in feed-forward operations [34,35] and subsequent computations to be performed in a fault-tolerant way [36]. Cluster states have the property that as the number of qubits increases, violation of the Bell inequalities increases exponentially [37]. Also, in noisy environments, the lifetime of entanglement is independent of the number of qubits, while for GHZ states, the lifetime approaches zero with increasing qubit number [38,39]. This makes the cluster state worthy of more theoretical and experimental investigation.

We thank the Laboratory of Microfabrication, University of Science and Technology of China, Institute of Physics CAS and National Center for Nanoscience and Technology for the support of the sample fabrication. This research was supported by the National Basic Research Program (973) of China under Grant No. 2017YFA0304300, the Chinese Academy of Science, Alibaba Cloud and Science and Technology Committee of Shanghai Municipality. X.-B. Z. is supported by NSFC under Grants No. 11574380. H.-H. W. is supported by NSFC under Grants No. 11434008.

[1] R. Horodecki, P. Horodecki, M. Horodecki, and K. Horodecki, Rev. Mod. Phys. **81**, 865 (2009).
[2] P. Shadbolt, J. C. Mathews, A. Laing, and J. L. O'brien, Nat. Phys. **10**, 278 (2014).
[3] T. D. Ladd, F. Jelezko, R. Laflamme, Y. Nakamura, C. Monroe, and J. L. OBrien, Nature (London) **464**, 45 (2010).
[4] I. Buluta and F. Nori, Science **326**, 108 (2009).
[5] H. J. Kimble, Nature (London) **453**, 1023 (2008).
[6] V. Giovannetti, S. Lloyd, and L. Maccone, Nat. Photonics **5**, 222 (2011).
[7] O. Gühne and G. Tóth, Phys. Rep. **474**, 1 (2009).
[8] C. Song, K. Xu, W. Liu, C.-p. Yang, S.-B. Zheng, H. Deng, Q. Xie, K. Huang, Q. Guo, L. Zhang *et al.*, Phys. Rev. Lett. **119**, 180511 (2017).
[9] T. Monz, P. Schindler, J. T. Barreiro, M. Chwalla, D. Nigg, W. A. Coish, M. Harlander, W. Hänsel, M. Hennrich, and R. Blatt, Phys. Rev. Lett. **106**, 130506 (2011).
[10] X.-L. Wang, Y.-H. Luo, H.-L. Huang, M.-C. Chen, Z.-E. Su, C. Liu, C. Chen, W. Li, Y.-Q. Fang, X. Jiang *et al.*, Phys. Rev. Lett. **120**, 260502 (2018).
[11] N. Friis, O. Marty, C. Maier, C. Hempel, M. Holzäpfel, P. Jurcevic, M. B. Plenio, M. Huber, C. Roos, R. Blatt *et al.*, Phys. Rev. X **8**, 021012 (2018).
[12] J. Zhang, G. Pagano, P. W. Hess, A. Kyprianidis, P. Becker, H. Kaplan, A. V. Gorshkov, Z.-X. Gong, and C. Monroe, Nature (London) **551**, 601 (2017).
[13] H. Bernien, S. Schwartz, A. Keesling, H. Levine, A. Omran, H. Pichler, S. Choi, A. S. Zibrov, M. Endres, M. Greiner *et al.*, Nature (London) **551**, 579 (2017).
[14] R. Harris, Y. Sato, A. Berkley, M. Reis, F. Altomare, M. Amin, K. Boothby, P. Bunyk, C. Deng, C. Enderud *et al.*, Science **361**, 162 (2018).

[15] Y. Wang, Y. Li, Z.-q. Yin, and B. Zeng, npj Quantum Inf. **4**, 46 (2018).
[16] R. Raussendorf and H. J. Briegel, Phys. Rev. Lett. **86**, 5188 (2001).
[17] H. J. Briegel, D. E. Browne, W. Dür, R. Raussendorf, and M. Van den Nest, Nat. Phys. **5**, 19 (2009).
[18] S. Boixo, S. V. Isakov, V. N. Smelyanskiy, R. Babbush, N. Ding, Z. Jiang, M. J. Bremner, J. M. Martinis, and H. Neven, Nat. Phys. **14**, 595 (2018).
[19] J. Koch, T. M. Yu, J. Gambetta, A. A. Houck, D. Schuster, J. Majer, A. Blais, M. H. Devoret, S. M. Girvin, and R. J. Schoelkopf, Phys. Rev. A **76**, 042319 (2007).
[20] R. Barends, J. Kelly, A. Megrant, A. Veitia, D. Sank, E. Jeffrey, T. C. White, J. Mutus, A. G. Fowler, B. Campbell *et al.*, Nature (London) **508**, 500 (2014).
[21] See Supplemental Material at http://link.aps.org/supplemental/10.1103/PhysRevLett.122.110501 for details about gate generation and optimization, the discussion about TLSs, the method for determining the lower bound of LC states and other related experiments, which includes Refs. [22–29].
[22] F. W. Strauch, P. R. Johnson, A. J. Dragt, C. J. Lobb, J. R. Anderson, and F. C. Wellstood, Phys. Rev. Lett. **91**, 167005 (2003).
[23] L. Dicarlo, J. M. Chow, J. M. Gambetta, L. S. Bishop, B. R. Johnson, D. I. Schuster, J. Majer, A. Blais, L. Frunzio, S. M. Girvin, and R. J. Schoelkopf, Nature (London) **460**, 240 (2009).
[24] L. DiCarlo, M. D. Reed, L. Sun, B. R. Johnson, J. M. Chow, J. M. Gambetta, L. Frunzio, S. M. Girvin, M. H. Devoret, and R. J. Schoelkopf, Nature (London) **467**, 574 (2010).
[25] T. Yamamoto, M. Neeley, E. Lucero, R. C. Bialczak, J. Kelly, M. Lenander, M. Mariantoni, A. D. O'Connell, D. Sank, H. Wang, M. Weides, J. Wenner, Y. Yin, A. N. Cleland, and J. M. Martinis, Phys. Rev. B **82**, 184515 (2010).
[26] J. Kelly *et al.*, Phys. Rev. Lett. **112**, 240504 (2014).
[27] J. M. Martinis and M. R. Geller, Phys. Rev. A **90**, 022307 (2014).
[28] M. Steffen, M. Ansmann, R. C. Bialczak, H. Katz, E. Lucero, R. McDermott, M. Neeley, E. M. Weig, A. N. Cleland, and J. M. Martinis, Science **313**, 1423 (2006).
[29] Y. Zheng, C. Song, M.-C. Chen, B. Xia, W. Liu, Q. Guo, L. Zhang, D. Xu, H. Deng, K. Huang, Y. Wu, Z. Yan, D. Zheng, L. Lu, J.-W. Pan, H. Wang, C.-Y. Lu, and X. Zhu, Phys. Rev. Lett. **118**, 210504 (2017).
[30] G. Tóth and O. Gühne, Phys. Rev. Lett. **94**, 060501 (2005).
[31] B. Jungnitsch, T. Moroder, and O. Gühne, Phys. Rev. Lett. **106**, 190502 (2011).
[32] E. Knill, D. Leibfried, R. Reichle, J. Britton, R. B. Blakestad, J. D. Jost, C. Langer, R. Ozeri, S. Seidelin, and D. J. Wineland, Phys. Rev. A **77**, 012307 (2008).
[33] D. C. McKay, S. Sheldon, J. A. Smolin, J. M. Chow, and J. M. Gambetta, arXiv:1712.06550.
[34] R. Prevedel, P. Walther, F. Tiefenbacher, P. Böhi, R. Kaltenbaek, T. Jennewein, and A. Zeilinger, Nature (London) **445**, 65 (2007).
[35] G. Vallone, E. Pomarico, F. De Martini, and P. Mataloni, Phys. Rev. Lett. **100**, 160502 (2008).
[36] R. Raussendorf, J. Harrington, and K. Goyal, New J. Phys. **9**, 199 (2007).
[37] O. Gühne, G. Tóth, P. Hyllus, and H. J. Briegel, Phys. Rev. Lett. **95**, 120405 (2005).
[38] H. J. Briegel and R. Raussendorf, Phys. Rev. Lett. **86**, 910 (2001).
[39] W. Dür and H.-J. Briegel, Phys. Rev. Lett. **92**, 180403 (2004).